Progress In Electromagnetics Research B, Vol. 55, 1–21, 2013

IMPACT OF FINITE GROUND PLANE EDGE DIFFRACTIONS ON RADIATION PATTERNS OF APERTURE ANTENNAS

Nafati A. Aboserwal, Constantine A. Balanis*, and Craig R. Birtcher

School of Electrical, Computer and Energy Engineering, Arizona State University, Tempe, AZ 85287-5706, USA

Abstract—In this study, the impact of finite ground plane edge diffractions on the amplitude patterns of aperture antennas is examined. The Uniform Theory of Diffraction (UTD) and the Geometrical Optics (GO) methods are utilized to calculate the amplitude patterns of a conical horn, and rectangular and circular waveguide apertures mounted on square and circular finite ground planes. The electric field distribution over the antenna aperture is obtained by a modal method, and then it is employed to calculate the geometrical optics field using the aperture integration method. The UTD is then applied to evaluate the diffraction from the ground planes' edges. Far-zone amplitude patterns in the E and H planes are finally obtained by the vectorial summation of the GO and UTD fields. In this paper, to accurately predict the H-plane amplitude patterns of circular and rectangular apertures mounted on square ground planes, the E-plane edge diffractions need to be included because the E-plane edge diffractions are much more intense than those of the H-plane edge regular and slope diffractions. Validity of the analysis is established by satisfactory agreement between the predicted and measured data and those simulated by Ansoft's High Frequency Structure Simulator (HFSS). Good agreement is observed for all cases considered.

Received 27 August 2013, Accepted 18 September 2013, Scheduled 23 September 2013
* Corresponding author: Constantine A. Balanis (balanis@asu.edu).
Invited paper dedicated to the memory of Robert E. Collin.

1. INTRODUCTION

Aperture antennas are most commonly used at microwave frequencies. They are very practical for space applications, where they can be conveniently integrated on the surface of the spacecraft or aircraft without affecting its aerodynamic profile. They are also used as a feed element for large radio astronomy, satellite tracking, and communication dishes. Their openings are usually covered with a dielectric material to protect them from environmental conditions [1, 2]. Because of the aforementioned reasons, aperture antennas have become one of the important microwave antennas. An investigation of the impact of finite ground planes on aperture antenna performance will aid in understanding when the antenna is placed in more complex structures.

In this paper, the UTD method is utilized to calculate the far-zone amplitude patterns in the E and H planes, and to examine the impact of the square and circular ground plane edges on the amplitude patterns of a conical horn, and rectangular and circular waveguide antennas. A modal technique is used to calculate the electric field distribution over the antenna aperture. After the field distribution over the antenna aperture is obtained, the GO field can be easily calculated, and the UTD is employed to account for the diffracted fields from the edges of the ground plane. The main contributions of this paper are:

- Predict accurately the H-plane amplitude pattern of rectangular and circular apertures mounted on a ground plane with straight edges over a dynamic range of 0–60 dB. Previously the H-plane pattern has been computed using slope diffraction as the regular first-order diffraction in this plane is zero, but only over a dynamic range of 0–40 dB. However, slope diffraction is not sufficient for 0–60 dB dynamic range prediction and, as shown and contributed in this paper, diffractions from the edges of the E plane (which are parallel to the H plane) must be included for the H-plane pattern to compare favorably with measurements and simulations using HFSS.
- Compare the amplitude patterns of rectangular and circular apertures when mounted on square and circular ground planes. It is shown that along the symmetry axis in the back region (near and at $\theta = 180^\circ$) the patterns of the apertures, when they are mounted on a circular ground plane are, 10–13 dB more intense than the patterns of the same apertures, mounted on a square ground plane. The diameter of the circular ground plane is equal to the length of one side of the square ground plane. This difference is attributed to the formation of a "ring radiator" by the circular ground plane.

The analytical results are validated by comparing them with measurements and data simulated using Ansoft's HFSS [3]. Good agreement is observed for all the cases considered. Edge diffractions have a significant impact on the far side and back lobes but do not affect significantly the forward main lobe.

The organization of this paper is as follows. The geometrical optics method is briefly reviewed in Section 2, followed by a detailed description of the Uniform Theory of Diffraction in Section 3. In Section 4, radiation patterns calculated by the method of this paper are compared with measurements and numerical simulations. Finally, Section 5 concludes the paper. Throughout this paper, the time convention $\exp(j\omega t)$ is used, and it is suppressed.

2. GEOMETRICAL OPTICS

One of the most versatile and useful ray-based, high-frequency, techniques is the Geometrical Optics (GO). The Geometrical Optics ray field consists of direct, refracted, and reflected rays. It is well known that electromagnetic waves are physically continuous, in magnitude and phase, in the time and space domains. However, the geometrical optics has limitations in which the GO yields fields that are discontinuous across the shadow boundaries created by the geometry of the problem. GO is insufficient to describe completely the scattered field in practical applications due to the inaccuracies inherent to GO near the shadow boundaries and in the shadow zone. The radiated fields from aperture antennas are determined from a knowledge of the fields over the aperture of the antenna. The aperture fields become the sources of the radiated fields. This is a variation of the Huygens's principle which states that points on each wavefront become the sources of secondary spherical waves propagating outwards and whose superposition generates the next wavefront.

To find far-zone radiation characteristics of aperture antennas, the equivalence principle, in terms of equivalent current densities $\mathbf{J}_s$ and $\mathbf{M}_s$, can be utilized to represent the fields at the aperture of the antenna. When the antenna is not mounted on an infinite ground plane, an approximate equivalent is utilized in terms of both $\mathbf{J}_s$ and/or $\mathbf{M}_s$ [1]. When the antenna is mounted on an infinite ground plane, an exact equivalent is formed, utilizing only $\mathbf{M}_s$ expressed in terms of the tangential electric fields at the aperture [1].

Aperture antennas are usually excited by waveguides. For rectangular and circular aperture antennas, rectangular and circular waveguides are, respectively, used as feeds. An analytical study of the radiation characteristics of an aperture antenna, mounted on a ground

plane, requires accurate amplitude and phase expressions for the fields over the aperture. For the conical horn, a spherical phase term, representing the spherical phase variations over the aperture, is added to the waveguide-derived fields as if the aperture fields have emanated from a virtual source located at the vertex inside the waveguide [1].

The total fields in space are a combination of the components of GO and UTD. Depending on the geometry of the problem, UTD can provide other diffraction mechanisms (slope diffraction, equivalent current contribution) to increase the prediction accuracy. The total field in space at a give observation point can be represented by

$$\mathbf{E_{Total}} = \mathbf{E_{Direct}} + \mathbf{E_{Reflected}} + \mathbf{E_{Diffracted}}$$
$$\mathbf{E_{Total}} = \mathbf{E_{GO}} + \mathbf{E_{UTD}}$$

where GO represents the direct and reflected fields and UTD represents the diffracted fields. By summing vectorially the GO and UTD fields, the total field is computed at a given observation point.

Since the UTD is an extension of Geometrical Optics used to describe diffraction phenomena, we will first briefly review the Geometrical Optics fields of a conical horn mounted on an infinite ground plane. In addition, the Geometrical Optics fields radiated by rectangular and circular waveguides, mounted on an infinite ground plane, will be illustrated.

2.1. Infinite Ground Plane Solution of Conical Horn Antenna

As shown in Figure 1(a), a circular aperture of radius a of a conical horn antenna is mounted on a perfectly electric conducting (PEC) ground plane. The fields over the aperture of the horn are those of a TE_{11} mode for a circular waveguide. The only difference is the inclusion of a complex exponential term which represents the spherical phase distribution over the aperture. Throughout this the paper, the spherical coordinate system, shown in Figure 1(c), is used to represent the radiated field from the antenna.

To find the radiation characteristics of a conical horn, the equivalence principle, in terms of an equivalent magnetic current density $\mathbf{M}_s$, can be utilized to represent the fields at the aperture of the horn. Because the horn aperture is mounted on an infinite ground plane, only the equivalent magnetic current density is nonzero over the aperture [1, 4]. By using the aperture integration method, the far-zone fields for the conical horn antenna on an infinite ground plane are given by

$$E_\theta = j\frac{k}{2\pi r}e^{-jkr}\sin\phi L_\theta \tag{1}$$

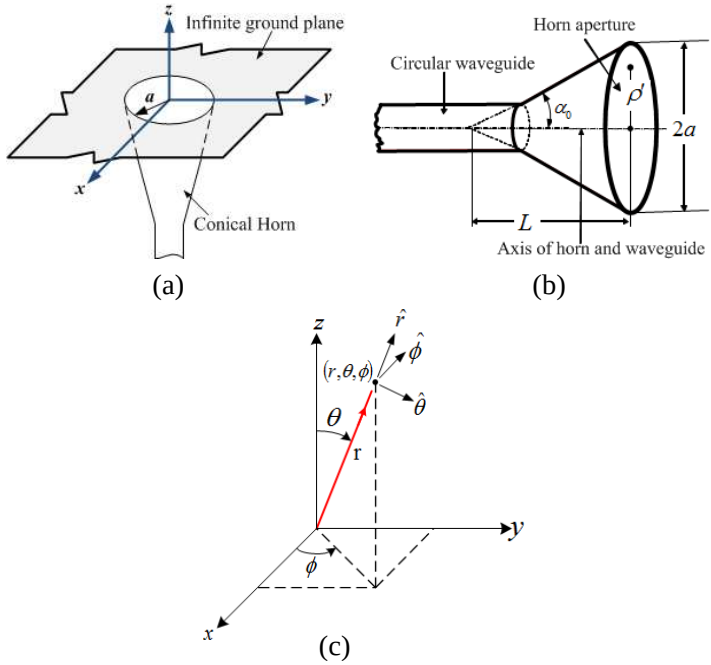

Figure 1. Geometry of a conical horn antenna, (a) mounted on an infinite ground plane, (b) in free space, and (c) the spherical coordinate system.

$$E_\phi = j\frac{k}{2\pi r}e^{-jkr}\cos\theta\cos\phi\ L_\phi \tag{2}$$

where

$$L_\theta = \int_0^a \left[\rho' J_0\left(k_\rho\rho'\right)J_0\left(k\rho'\sin\theta\right) - \rho' J_2\left(k_\rho\rho'\right)J_2\left(k\rho'\sin\theta\right)\right]e^{-jk\delta(\rho')}d\rho' \tag{3}$$

$$L_\phi = \int_0^a \left[\rho' J_0\left(k_\rho\rho'\right)J_0\left(k\rho'\sin\theta\right) + \rho' J_2\left(k_\rho\rho'\right)J_2\left(k\rho'\sin\theta\right)\right]e^{-jk\delta(\rho')}d\rho' \tag{4}$$

and $\delta(\rho')$ is *the spherical path length term* [5, 6]. $k = 2\pi/\lambda$, λ is the free-space wavelength, $k_\rho = 1.8412/a$, $J_m(x)$ is the Bessel function of first kind of order m, (r, θ, ϕ) are the spherical polar coordinates, and the ρ' indicates the radial cylindrical coordinate of the equivalent excitation source over the antenna aperture as shown in Figure 1(b). These components, (1)–(4), represent the fields radiated in the forward region $(0 \le \theta \le \pi/2)$.

2.2. Infinite Ground Plane Solution of Rectangular and Circular Waveguide Antennas

The geometry of a rectangular waveguide of dimensions a and b, and a circular waveguide of radius a, mounted on an infinite ground plane, are shown in Figure 2. The coordinate system is located at the center of the aperture. The fields over the aperture are assumed to be the TE_{10}-mode fields for the rectangular waveguide and the TE_{11}-mode fields for the circular waveguide.

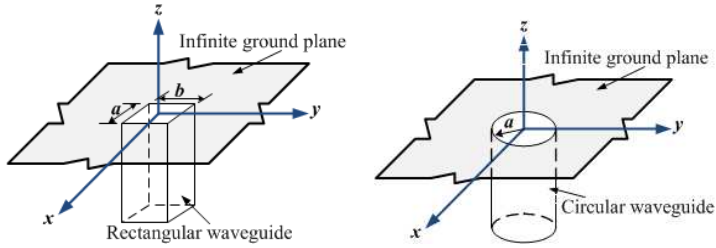

Figure 2. Geometry of (a) rectangular and (b) circular waveguides mounted on an infinite ground plane.

These fields are assumed to be known and are produced by the waveguide which feeds the aperture antenna mounted on the infinite ground plane. The fields radiated from the aperture can be computed by using the field equivalence principle [1], which states that the aperture fields may be replaced by equivalent electric and magnetic surface currents whose radiated fields can then be calculated using the techniques of Section 12.2 of [1].

The far-zone fields radiated by waveguides mounted on an infinite ground plane can be written as [1]

$$E_\theta = \frac{-jkabE_0e^{-jkr}}{4r}\sin\phi\frac{\cos X}{X^2-\left(\frac{\pi}{2}\right)^2}\frac{\sin Y}{Y} \tag{5}$$

$$E_\phi = \frac{-jkabE_0e^{-jkr}}{4r}\cos\theta\cos\phi\frac{\cos X}{X^2-\left(\frac{\pi}{2}\right)^2}\frac{\sin Y}{Y} \tag{6}$$

for the rectangular waveguide, and

$$E_\theta = \frac{jkaE_0e^{-jkr}}{r}\sin\phi J_1(\chi'_{11})\frac{J_1(ka\sin\theta)}{ka\sin\theta} \tag{7}$$

$$E_\phi = \frac{jkaE_0e^{-jkr}}{r}\cos\theta\cos\phi J_1(\chi'_{11})\frac{J'_1(ka\sin\theta)}{1-\left(\frac{ka\sin\theta}{\chi'_{11}}\right)^2} \tag{8}$$

for the circular waveguide, where $X = \frac{ka}{2}\sin\theta\cos\phi$, $Y = \frac{kb}{2}\sin\theta\sin\phi$, $\chi'_{11} = 1.8412$, $J_m(x)$ is the Bessel function of first kind of order m, $J'_m(x)$ is the derivative of $J_m(x)$ with respect to the entire argument x, and E_0 is the normalized amplitude of the incident electric field.

3. GEOMETRICAL THEORY OF DIFFRACTION FOR AN EDGE ON A PERFECTLY CONDUCTING SURFACE

As is well known, the Geometrical Optics has some limitations because it does not predict the fields in the shadow region. Also, GO is inaccurate in the vicinity of the shadow boundaries. The GO predicts zero diffracted fields everywhere and zero direct and reflected fields in the shadow region. Therefore, the Geometrical Theory of Diffraction (GTD) is required to overcome these deficiencies. The GTD supplements and enhances Geometrical Optics by adding contributions due to edge diffraction at perfectly conducting edges. The introduction of the Geometrical Theory of Diffraction by Keller [7] and its modified version, the Uniform Theory of Diffraction (UTD), introduced by Kouyoumjian and Pathak [8], have proved to be very valuable in solving antenna problems that otherwise may be intractable. The UTD corrects for the singularities of the diffracted field along the incident and reflection shadow boundaries. The application of this theory on a $\lambda/4$ monopole mounted on infinitely thin, perfectly conducting, finite square and circular ground planes has been examined in [4]. However, the edges may have significant thickness in terms of wavelengths at higher microwaves frequencies. The impact of the thick finite ground plane on the radiation patterns of a $\lambda/4$ monopole has been studied by Ibrahim and Stephenson in [9]. The uniform theory of diffraction was used in [10] to calculate the edge diffracted fields from the finite ground plane of a microstrip antenna. These techniques have also been applied to horn antennas in free space [11–19]. In addition, the radiation patterns of an infinitesimal monopole mounted on the tip of a perfectly conducting, finite length cone was calculated using diffraction techniques [20].

In this paper, the UTD analysis of the far-zone E-plane and H-plane amplitude patterns of a conical horn, and rectangular and circular waveguide antennas mounted on finite square and circular ground planes is presented. The study enables one to predict accurately the far-zone E- and H-plane amplitude patterns over the main beam, near and far sidelobes, and backlobes. The fields radiated by these antennas when mounted on infinite ground planes, which are well known, are supplemented by the fields diffracted at the edges of the finite ground planes. The UTD is utilized to calculate the diffracted

field components. The circular edge of the circular ground plane has a caustic along its axis, and the UTD predicts an infinite field there, which physically does not exist. This deficiency can be overcome by the use of equivalent edge currents [21]. These currents flow along the edge, and their integration around the circular rim produces a finite field value in the caustic region.

3.1. Diffracted Field Solution

The total field can be calculated by summing the GO field and diffracted fields from the edges of the ground plane. According to the Uniform Theory of Diffraction [4], the diffracted field can be expressed as

$$\bar{E}^d = \bar{E}^i(Q_d) \cdot \bar{\bar{D}} \sqrt{\frac{\rho_c}{s(\rho_c + s)}} \exp(-jks) \tag{9}$$

where $\bar{E}^i(Q_d)$ is the electric field incident at a point Q_d on the edge, and $\bar{\bar{D}}$ is the dyadic diffraction coefficient $\bar{\bar{D}} = -\hat{\beta}_0'\hat{\beta}_0 D^s - \hat{\phi}'\hat{\phi} D^h$, where D^s and D^h are, respectively, the soft and hard polarization diffraction coefficients. ρ_c is the distance between the caustic at the edge and the second caustic of the diffracted ray. The unit vectors $\hat{\beta}_0'$, $\hat{\beta}_0$, $\hat{\phi}'$, $\hat{\phi}$, together with ρ_c, are illustrated in Figures 13–31 of [4]. ρ_c is represented by

$$\frac{1}{\rho_c} = \frac{1}{\rho_e^i} - \frac{\hat{n} \cdot (\hat{s}' - \hat{s})}{\rho_g \sin^2 \beta_0'} \tag{10}$$

where ρ_e^i is the radius of curvature of the incident wavefront at Q_d taken in the plane containing the incident ray and the unit vector tangent to the edge at Q_d; ρ_g is the radius of curvature of the edge at Q_d; $\hat{n}$ is the unit normal to the edge directed away from the center of curvature; β_0' is the angle between the incident ray and the tangent to the edge at Q_d; and $\hat{s}'$ and $\hat{s}$ are, respectively, unit vectors in the direction of incidence and diffraction. The soft and hard polarization diffraction coefficients are represented by [4]

$$\begin{aligned} D^{s,h} = \frac{-e^{-j\pi/4}}{2n\sqrt{2\pi k}\sin\beta_0'} \Bigg(\Bigg\{ & \cot\left[\frac{\pi + (\xi^-)}{2n}\right] F[kL^i g^+(\xi^-)] \\ & + \cot\left[\frac{\pi - (\xi^-)}{2n}\right] F\left[kL^i g^-(\xi^-)\right] \Bigg\} \mp \Bigg\{ \cot\left[\frac{\pi + (\xi^+)}{2n}\right] F\left[kL^{rn} g^+(\xi^+)\right] \\ & + \cot\left[\frac{\pi - (\xi^+)}{2n}\right] F\left[kL^{ro} g^-(\xi^+)\right] \Bigg\} \Bigg) \end{aligned} \tag{11}$$

where $F(x)$ is the Fresnel integral, given by

$$F(x) = 2j\sqrt{x}e^{jx}\int_{\sqrt{x}}^{\infty} e^{-jt^2}dt \tag{12}$$

$g^{\pm}(\xi) = 1 + \cos(2n\pi N^{\pm} - \xi)$, $\xi^{\pm} = \phi \pm \phi'$; $N\pm$ is the positive or negative integer or zero which most nearly satisfies

$$2n\pi N^{+} - \xi = +\pi$$
$$2n\pi N^{-} - \xi = -\pi$$

n is a parameter that determines the wedge angle. For the present problem, $n = 2$ where the wedge has zero interior angle. For the definitions of distance parameters (L^i, L^{rn}, and L^{ro}), refer to [4]. Because the intersecting surfaces forming the edges are plane surfaces, the distance parameters are equal, that is,

$$L^i = L^{ro} = L^{rn} = L \tag{13}$$

For far-field observations, L is given by

$$L \approx s' \quad s \gg s' \tag{14}$$

where s' is the source distance to the diffracting points in the E and H planes.

3.2. Edge Diffraction of Aperture Antennas Mounted on Finite Ground Planes

In this section, two geometries, aperture antennas mounted on square and circular ground planes, are treated similarly. Far-zone E- and H-plane amplitude patterns are analytically calculated for the square and circular ground planes following the procedure as described in the previous section. Also, it should be noted that since the incident field is at grazing incidence, the total GO field is multiplied by a factor of 1/2 [1, 4]. To investigate the influence of the ground plane geometry on the E- and H-plane amplitude patterns, a comparison of square and circular ground planes, where the side of the square is equal to the diameter of the circular, is carried out.

The incident field at points Q_{d1} and Q_{d2}, as shown in Figure 3, is found from (1)–(6) after substituting $\theta = \pi/2$ and $r = w$; w is the half width of the square ground plane or the radius of the circular ground plane. ρ_{c1} and ρ_{c2} are the distances between the caustic at the diffraction points (Q_{d1} and Q_{d2}) and second caustic of diffracted ray, and they are found from (10). For the aperture antennas mounted on a square ground plane:

$$\rho_{c1} = \rho_{c2} = w \tag{15}$$

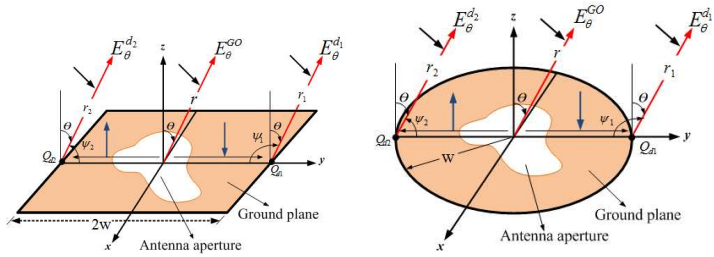

Figure 3. Diffraction mechanism by edges of (a) square and (b) circular ground planes.

and for the circular ground plane:

$$\rho_{c1} = \frac{w}{\sin\theta} \tag{16}$$

$$\rho_{c2} = -\frac{w}{\sin\theta} \tag{17}$$

The distance parameters L_1 and L_2 of (14) are the same for both the square and circular ground planes at the diffraction points Q_{d1} and Q_{d2}:

$$L_1 = L_2 = w \tag{18}$$

The diffracted field components from diffracting points Q_{d1} and Q_{d2}, for either the square or the circular ground planes, are:

$$E_\theta^{d_1} = \frac{1}{2} E_\theta^i \left(w, \frac{\pi}{2}, \frac{\pi}{2}\right) D^h \left(L_1, \psi_1, 0, \frac{\pi}{2}, 2\right) \sqrt{\rho_{c1}} \frac{e^{-jkr_1}}{r_1} \tag{19}$$

$$E_\theta^{d_2} = \frac{1}{2} E_\theta^i \left(w, \frac{\pi}{2}, \frac{\pi}{2}\right) D^h \left(L_2, \psi_2, 0, \frac{\pi}{2}, 2\right) \sqrt{\rho_{c2}} \frac{e^{-jkr_2}}{r_2} \tag{20}$$

for the E-plane diffracted field, and

$$E_\phi^{d_1} = \frac{1}{2} E_\phi^i \left(w, \frac{\pi}{2}, 0\right) D^s \left(L_1, \psi_1, 0, \frac{\pi}{2}, 2\right) \sqrt{\rho_{c1}} \frac{e^{-jkr_1}}{r_1} \tag{21}$$

$$E_\phi^{d_2} = \frac{1}{2} E_\phi^i \left(w, \frac{\pi}{2}, 0\right) D^s \left(L_2, \psi_2, 0, \frac{\pi}{2}, 2\right) \sqrt{\rho_{c2}} \frac{e^{-jkr_2}}{r_2} \tag{22}$$

for the H-plane diffracted field, where

$$\psi_1 = \frac{\pi}{2} + \theta \qquad (0 \le \theta \le \pi) \tag{23}$$

$$\begin{aligned} \psi_2 &= \frac{\pi}{2} - \theta \qquad \left(0 \le \theta \le \frac{\pi}{2}\right) \\ &= \frac{5\pi}{2} - \theta \qquad \left(\frac{\pi}{2} < \theta \le \pi\right) \end{aligned} \tag{24}$$

For far-field observations

$$r_1 \simeq r - w\cos\left(\frac{\pi}{2}-\theta\right) = r - w\sin\theta \tag{25}$$

$$r_2 \simeq r + w\cos\left(\frac{\pi}{2}-\theta\right) = r + w\sin\theta \tag{26}$$

for phase terms, and

$$r_1 \simeq r_2 \simeq r \tag{27}$$

for amplitude terms.

Therefore, the diffracted fields from the diffracting points Q_{d1} and Q_{d2} reduce to

$$E_\theta^{d_1} = \frac{1}{2}E_\theta^i\Big(w,\frac{\pi}{2},\frac{\pi}{2}\Big)D^h\Big(L_1,\psi_1,0,\frac{\pi}{2},2\Big)\sqrt{\rho_{c1}}e^{+jw\sin\theta}\frac{e^{-jkr}}{r} \tag{28}$$

$$E_\theta^{d_2} = \frac{1}{2}E_\theta^i\Big(w,\frac{\pi}{2},\frac{\pi}{2}\Big)D^h\Big(L_2,\psi_2,0,\frac{\pi}{2},2\Big)\sqrt{\rho_{c2}}e^{-jw\sin\theta}\frac{e^{-jkr}}{r} \tag{29}$$

for the far-zone E plane, and

$$E_\phi^{d_1} = \frac{1}{2}E_\phi^i\Big(w,\frac{\pi}{2},0\Big)D^s\Big(L_1,\psi_1,0,\frac{\pi}{2},2\Big)\sqrt{\rho_{c1}}e^{+jw\sin\theta}\frac{e^{-jkr}}{r} \tag{30}$$

$$E_\phi^{d_2} = \frac{1}{2}E_\phi^i\Big(w,\frac{\pi}{2},0\Big)D^s\Big(L_2,\psi_2,0,\frac{\pi}{2},2\Big)\sqrt{\rho_{c2}}e^{-jw\sin\theta}\frac{e^{-jkr}}{r} \tag{31}$$

for the far-zone H plane.

So far, the diffraction effects of this study are accounted for by using only the diffraction which depends on the magnitude of the incident field. However, this indicates that the diffracted field would be zero if the incident field is zero. Physically, the diffracted fields do not go to zero. Thus a second-order diffraction, due to the rapid change of the GO field near the edge, can be incorporated into the analysis. In the H plane for the square and circular ground planes, it is noted that the first-order diffracted fields are zero because the electric field on the surface of a conductor wedge vanishes for a grazing incident wave. Therefore, the slope diffracted fields, second-order diffracted fields, from the diffraction points are given by [4]

$$E_\theta^{slope} = \frac{1}{jk}\left[\frac{\partial E_\theta^i(Q_d)}{\partial n}\right]\left(\frac{\partial D^h}{\partial \phi'}\right)\sqrt{\frac{\rho_c}{s(\rho_c+s)}}\,e^{-jks} \tag{32}$$

$$E_\phi^{slope} = \frac{1}{jk}\left[\frac{\partial E_\phi^i(Q_d)}{\partial n}\right]\left(\frac{\partial D^s}{\partial \phi'}\right)\sqrt{\frac{\rho_c}{s(\rho_c+s)}}\,e^{-jks} \tag{33}$$

where

$\frac{\partial E_\theta^i}{\partial n}|_{Q_d} = \hat{n}\cdot\nabla E_\theta^i|_{Q_d} = -\frac{1}{s'}\frac{\partial E_\theta^i}{\partial \phi'}|_{Q_d}$ = slope of incident field for hard polarization.

$\frac{\partial E_\phi^i}{\partial n}|_{Q_d} = \hat{n} \cdot \nabla E_\phi^i|_{Q_d} = -\frac{1}{s'}\frac{\partial E_\phi^i}{\partial \phi'}|_{Q_d}$ = slope of incident field for soft polarization.

$\hat{n}$ is unit normal in ϕ' direction.

s' is the distance from the aperture center to the diffraction point.

s is the distance from the diffraction point to the observation point.

$\frac{\partial D^{h,s}}{\partial \phi'}$ = slope diffraction coefficient for hard and soft polarization, respectively, given by

$$\begin{aligned} D_{slope}^{s,h} = \frac{-e^{-j\pi/4}}{2n^2\sqrt{2\pi k}\sin\beta_0'} \Bigg(\Bigg\{ & \csc^2\left[\frac{\pi+(\xi^-)}{2n}\right] F_s\left[kLg^+\left(\xi^-\right)\right] \\ & - \csc^2\left[\frac{\pi-(\xi^-)}{2n}\right] F_s[kLg^-(\xi^-)] \Bigg\} \\ & \pm \Bigg\{ \csc^2\left[\frac{\pi+(\xi^+)}{2n}\right] F_s\left[kLg^+\left(\xi^+\right)\right] \\ & - \csc^2\left[\frac{\pi-(\xi^+)}{2n}\right] F_s[kLg^-(\xi^+)] \Bigg\} \Bigg) \end{aligned} \tag{34}$$

where

$$F_s(x) = 2jx[1 - F(x)] \tag{35}$$

and $F(x)$ is presented by (12).

Due to the circular symmetry of the circular ground plane's edge, the edge behaves as a continuous ring radiator which leads to the formation of a caustic where the diffracted field is infinity. Therefore, a caustic correction is needed for angles at and near the axis of the antenna. The UTD can be used to correct for this caustic. Ryan and Peters [21] showed that UTD equivalent currents can be used to correct for this caustic. Using this method, equivalent magnetic and electric currents are created on the edge of the aperture. Then radiation integrals are used to obtain fields due to these currents, which correct the diffracted fields at and near the symmetry axis of the antenna. The electric and magnetic equivalent currents take the form of

$$I_\phi^e = -\frac{\sqrt{8\pi k}}{\eta k} e^{-j\pi/4} D^s E_\phi^i(Q_d) \tag{36}$$

$$I_\phi^m = -\frac{\sqrt{8\pi k}}{k} e^{-j\pi/4} D^h E_\theta^i(Q_d) \tag{37}$$

The fields radiated by each of the equivalent currents can be obtained using techniques of Chapter 5 of [1]. Thus the radiated field

for a loop carrying an electric current I^e are given by

$$E_\theta^e = -\frac{j\omega\mu a}{4\pi r}\cos\theta e^{-jkr}\int_0^{2\pi} I^e(\phi')\sin(\phi-\phi')e^{jka\cos(\phi-\phi')\sin\theta}d\phi' \quad (38)$$

$$E_\phi^e = -\frac{j\omega\mu a}{4\pi r}e^{-jkr}\int_0^{2\pi} I^e(\phi')\cos(\phi-\phi')e^{jka\cos(\phi-\phi')\sin\theta}d\phi' \quad (39)$$

The duality theorem can be applied to obtain the fields radiated by a magnetic current I^m, rather than an electric current I^e, and it leads to

$$E_\theta^m = -\eta\frac{j\omega\epsilon a}{4\pi r}e^{-jkr}\int_0^{2\pi} I^m(\phi')\cos(\phi-\phi')e^{jka\cos(\phi-\phi')\sin\theta}d\phi' \quad (40)$$

$$E_\phi^m = \eta\frac{j\omega\epsilon a}{4\pi r}\cos\theta e^{-jkr}\int_0^{2\pi} I^m(\phi')\sin(\phi-\phi')e^{jka\cos(\phi-\phi')\sin\theta}d\phi' \quad (41)$$

Now, numerically integrating (38)–(41), corrected diffracted fields are obtained at and near the symmetry axis of the antenna.

The electric current is zero because the incident field (GO field) is zero at the edge. Therefore, the radiated fields of the electric current are zero. The corrected diffracted fields in the E and H planes due to a magnetic current around the ground edge are obtained at and near the symmetry axis of the antenna by computing numerically (40)–(41).

For the square ground plane, the slope diffraction does not significantly improve the radiation pattern in the backlobe region of the H-plane amplitude radiation pattern. Therefore, one needs to include the contributions from the E-plane edge diffractions because the E-plane edge diffractions have a much greater magnitude than those of the H-plane edge diffractions. This contribution can be calculated by using the equivalent current method that was described previously.

4. RESULTS AND VALIDATION: PREDICTIONS, SIMULATIONS AND MEASUREMENTS

All measurements were performed in the ElectroMagnetic Anechoic Chamber (EMAC) facility at Arizona State University. Models for the square and circular ground planes with rectangular and circular aperture antennas mounted at the center have been constructed. The ground planes are made of aluminum. A computer program was written in Matlab to calculate the normalized far-zone field amplitude patterns in the E and H planes for all cases considered in this work.

4.1. Conical Horn Antennas Mounted on Square and Circular Ground Planes

The width of the square ground plane and diameter of the circular ground plane are 12.2 in. Using a dynamic range of 100 dB, the agreement between theory, experiment, and HFSS simulations is good in the E and H planes for the X-band conical horn, having a total flare angle of 35° and an axial length $L = 8.2$ in. The frequency at which the measurements were preformed is 10.3 GHz. The diameter of the horn aperture is 5.36 in. The diameter of the waveguides (used for the measurements and HFSS simulations) is 0.9 in. Numerical and measured data are compared with simulated data based on Ansoft's High Frequency Structure Simulator (HFSS).

Figure 4 displays the far-zone E-plane amplitude patterns of the conical horn antenna mounted on the square and circular ground planes. The GO field in the forward region ($0 \leq \theta \leq \pi/2$) is calculated using (1) and (3) [because (2) vanishes in the E plane ($\phi = 90°$)]. The edge diffractions from the E-plane edges are included in the total amplitude pattern using (28) and (29). Very good agreement between theory, experiment and simulations is indicated; the total field consists of the GO and first-order diffracted fields. In addition, the fields associated with the equivalent currents of (38) and (40) are included for the circular ground planes.

The same comparison for the far-zone H-plane amplitude patterns

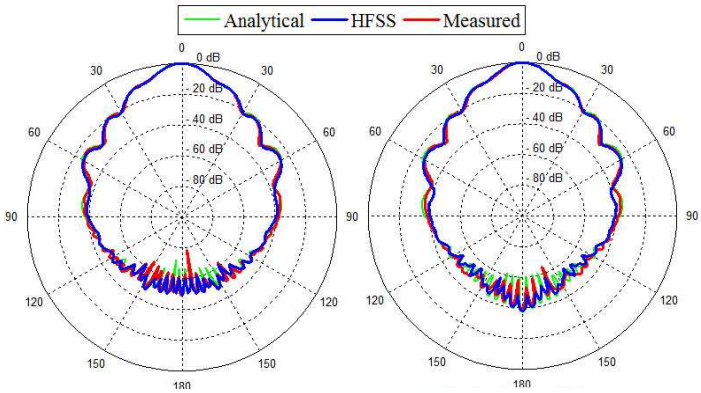

Figure 4. Far-zone E-plane amplitude patterns of an X-band conical horn antenna at 10.3 GHz ($L = 8.2$ in, $2\alpha_0 = 35°$, $2w = 12.2$ in) mounted on (a) square and (b) circular ground planes.

is illustrated in Figure 5. As shown in the figure, there is good agreement between predictions, measurements, and simulations; the total analytical field consists of the GO field given by (2) and (4) [because (1) vanishes in the H plane ($\phi = 0°$)], first-order diffracted fields obtained by using (30) and (31), and slope diffracted fields given by (33). The edge diffraction contributions using (30) and (31) on the overall amplitude pattern are zero where the amplitude pattern is similar to that of the infinite ground plane. In the back region ($\pi/2 \leq \theta \leq \pi$) of the H-plane pattern of antennas mounted on the square ground planes, the contributions from the E-plane edge diffractions should be included because the E-plane edge diffractions are more intense than those of the H-plane edge slope diffractions. Using (39) and (41), the fields associated with the equivalent currents are included for the circular ground planes to correct for the caustic formed by the diffracted fields at and near the symmetry axis of the antenna.

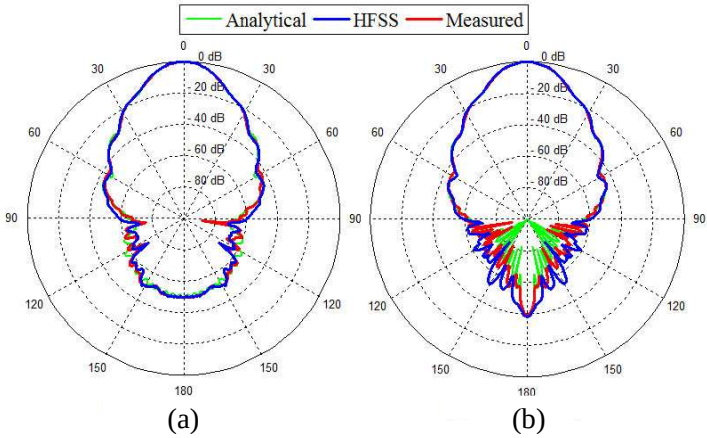

Figure 5. Far-zone H-plane amplitude patterns of an X-band conical horn antenna at 10.3 GHz ($L = 8.2$ in, $2\alpha_0 = 35°$, $2w = 12.2$ in) mounted on (a) square and (b) circular ground planes.

4.2. Rectangular and Circular Waveguides Mounted on Square and Circular Ground Planes

The rectangular and circular aperture antennas have been, respectively, excited by the TE_{10}-mode rectangular and the TE_{11}-mode circular waveguides. The width of the square ground plane and diameter of the circular ground plane is 12 in. Validity of the radiation pattern

analysis over the main beam and the near and far sidelobes presented above has been verified by calculating the far-zone E- and H-plane amplitude patterns of the aperture antennas. The frequency at which measurements are performed is 10 GHz. The dimensions of the rectangular aperture are $a = 0.9$ in and $b = 0.4$ in, and the diameter of the circular aperture is 0.938 in. A comparison between the predicted, measured, and simulated results has been made.

Figures 6 and 7 show, respectively, the far-zone E-plane amplitude patterns of rectangular and circular waveguide antennas mounted on the square and circular ground planes. Computed amplitude patterns are compared with experimental and simulated data, and a good agreement is indicated. The total field consists of the GO given by (5) and (7) for the rectangular and circular waveguides [because (6) and (8) vanish in the E plane ($\phi = 90°$)], respectively, and first-order diffracted fields from two diffraction points given by (28) and (29), depending on which ground plane is being considered. In addition, the diffracted fields associated with the equivalent currents for the circular ground planes are included at and near the symmetry axis of the antenna using (38) and (40).

Unlike the E-plane diffraction, there is no diffraction contribution from the H-plane edges because the incident waves at the diffraction points, given by (6) and (8) when $\theta = 90°$, are zero. However, second-order diffracted fields given by (33) from the diffraction points (Q_{d1} and Q_{d2}) are included to improve the total amplitude pattern

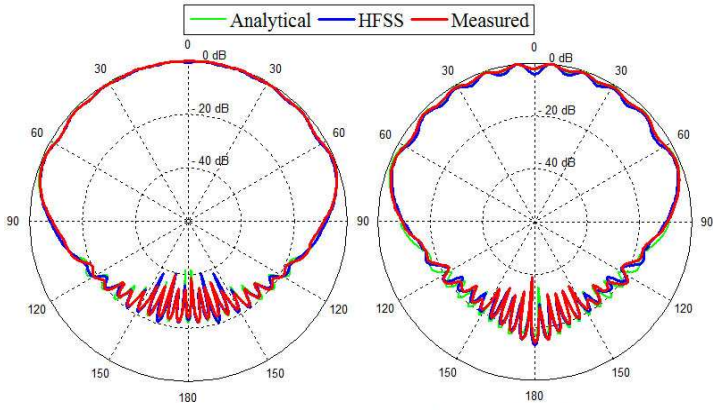

Figure 6. Far-zone E-plane amplitude patterns of a rectangular waveguide at 10 GHz ($a = 0.9$ in, $b = 0.4$ in, $2w = 12$ in), (a) square and (b) circular ground planes.

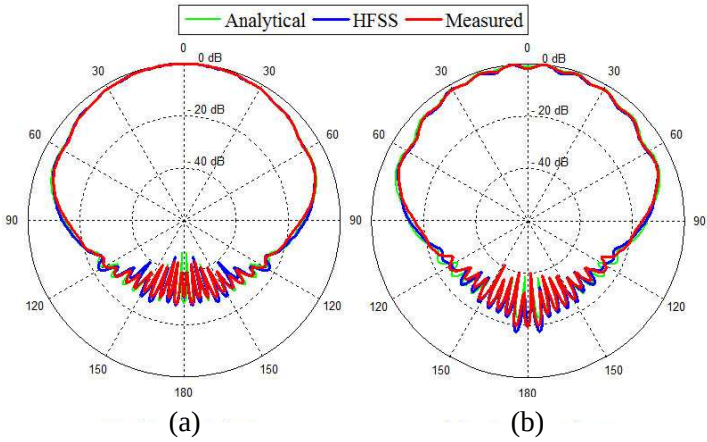

Figure 7. Far-zone E-plane amplitude patterns of a circular waveguide at 10 GHz ($a = 0.469$ in, $2w = 12$ in), (a) square and (b) circular ground planes.

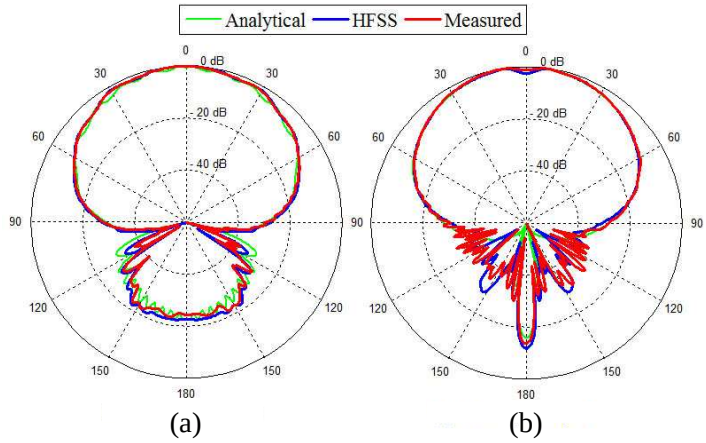

Figure 8. Far-zone H-plane amplitude patterns of a rectangular waveguide at 10 GHz ($a = 0.9$ in, $b = 0.4$ in, $2w = 12$ in), (a) square and (b) circular ground planes.

especially in the back region. The far-zone H-plane amplitude patterns of rectangular and circular waveguide antennas mounted on the square and circular ground planes, respectively, are shown in Figures 8 and 9. The GO fields are calculated using (6) and (8) for the rectangular and circular waveguides, respectively. Very good agreement between

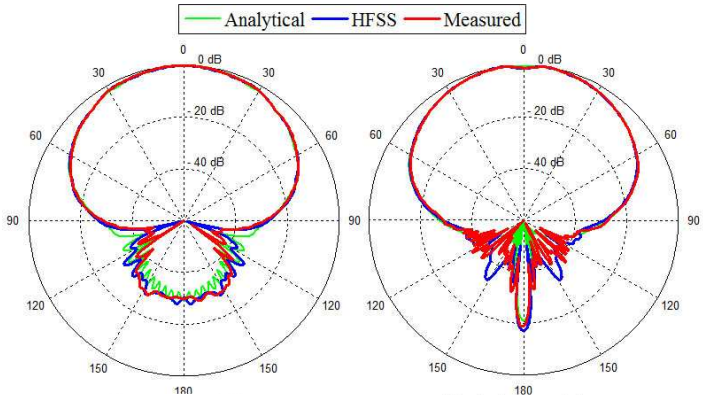

Figure 9. Far-zone H-plane amplitude patterns of a circular waveguide at 10 GHz ($a = 0.469$ in, $2w = 12$ in), (a) square and (b) circular ground planes.

theory, experiment and simulations is indicated; the total field consists of the GO, first-order diffracted, and slope diffracted fields. For the square ground plane, the contributions from the E-plane edge diffractions should be included to calculate the H-plane amplitude pattern. Also, the fields associated with the equivalent currents of (39) and (41) are included for the circular ground planes.

In all studied cases, it is very obvious that the magnitude of the amplitude pattern of the circular ground plane at and near the symmetry axis of the antenna, below the ground plane, is much larger compared to that of the square ground plane. Because of the symmetry of the circular ground plane, there is a ring radiator along the circular edge contributing about 10–13 dB greater at and near the symmetry axis of the circular ground plane, compared to that of the square ground plane.

5. CONCLUSIONS

In this investigation of conical horn, and rectangular and circular waveguide antennas mounted on finite ground planes, the edges of the finite ground plane influence the radiation patterns in the diffraction zone. This effect has been examined both analytically and experimentally. Two ground planes, square and circular, were chosen for this study. The study indicates that the finite ground plane does not

influence greatly the forward main pattern. Its primary impact appears in far side and back lobes regions. The aperture integration method, augmented by the Uniform Theory of Diffraction for the prediction of aperture antenna radiation, has been presented. The UTD edge diffractions are included for the finite ground plane in both the E- and H-plane predictions. In the E plane, single edge diffractions plus the direct GO field contribute to the total field. In the H plane, the total field consists of the direct GO field, single edge diffractions, slope diffracted field, and E-plane edge equivalent current field. In addition, the contributions of the electric and magnetic equivalent currents must be included for the circular ground plane to correct the caustics created by the the diffracted fields at and near the axis of the antenna. Numerical results obtained by our method are compared with measured data and those simulated by Ansoft's High Frequency Structure Simulator (HFSS). The measured and simulated results indicate that the predictions based on the analytical formulations, for both square and circular ground planes, are in very good agreement. This work demonstrates that the impact of the edges must be included in the calculation to obtain very accurate results of the amplitude patterns, especially for extended dynamic ranges.

For all studied cases, the H-plane electric field component of the incident field vanishes along the ground plane edge (grazing incidence). Thus, only diffraction by the E-plane edges contributes significantly to the E- and H-plane diffraction patterns. To obtain the far-zone E-plane amplitude pattern, only the diffraction from the midpoints of the E-plane edge contributes to the amplitude pattern. For the far-zone H-plane amplitude pattern, diffraction accruing at all points along the E-plane edge, non-normal and normal incidence of the incident GO fields at the edge, must be taken into consideration.

The discrepancies between the theoretical and measured results in the backward region of the far-zone E- and H-plane amplitude patterns can be attributed to the inability to accurately model the structure feeding the aperture antennas as well as the structure used to support the antenna during the measurements.

REFERENCES

1. Balanis, C. A., *Antenna Theory: Analysis and Design*, John Wiley and Sons, New Jersey, 2005.
2. Kraus, J. D. and R. J. Marhefka, *Antennas for All Applications*, McGraw-Hill, New York, 2002.
3. Online Available: http://www.ansoft.com/products/hf/hfss/Ansoft Corporation HFSS.

4. Balanis, C. A., *Advanced Engineering Electromagnetics*, John Wiley and Sons, New Jersey, 2012.
5. Aboserwal, N. A., C. A. Balanis, and C. R. Birtcher, "Conical horn: Gain and amplitude patterns," *IEEE Trans. Antennas Propagat.*, Vol. 61, No. 7, 3427–3433, Jul. 2013.
6. Love, A. W., *Electromagnetic Horn Antennas*, IEEE Press, New York, 1976.
7. Keller, J. B., "Geometrical theory of diffraction," *J. Opt. Soc. Amer.*, Vol. 52, 116–130, Feb. 1962.
8. Kouyoumjian, R. G. and P. H. Pathak, "A uniform geometrical theory of diffraction for an edge in a perfectly conducting surface," *Proceedings IEEE*, Vol. 62, No. 11, 1448–1461, Nov. 1974.
9. Ibrahim, H. M. and D. T. Stephenson, "Radiation patterns of a $\lambda/4$ monopole mounted on thick finite square and circular ground planes," *Int. J. Electronics*, Vol. 64, No. 3, 345–358, Jul. 1988.
10. Huang, J., "The finite ground plane effect on the microstrip antenna radiation patterns," *IEEE Trans. Antennas Propagat.*, Vol. 31, No. 4, 649–653, Jul. 1983.
11. Narasimhan, M. S. and M. Sheshadri, "GTD analysis of the radiation patterns of conical horns," *IEEE Trans. Antennas Propagat.*, Vol. 26, No. 6, 774–778, Nov. 1978.
12. Ali, M., S. Sanyal, and S. Park, "Analysis of horn radiation pattern using UTD edge and corner diffraction," *Progress In Electromagnetics Research M*, Vol. 17, 87–99, 2011.
13. Menendez, R. and S. W. Lee, "Analysis of rectangular horn antennas via uniform asymptotic theory," *IEEE Trans. Antennas Propagat.*, Vol. 30, No. 2, 241–250, Mar. 1982.
14. Narsimhan, M. S. and S. K. Rao, "GTD analysis of the near-field patterns of pyramidal horns," *Proceedings IEEE*, Vol. 126, No. 12, 1223–1226, Dec. 1979.
15. Balanis, C. A., "Pattern distortion due to edge diffractions," *IEEE Trans. Antennas Propagat.*, Vol 18, 561–563, Jul. 1970.
16. Ali, M. and S. Sanyal, "A finite edge GTD analysis of the H-plane horn radiation pattern," *Proceedings IEEE*, Vol. 58, No. 3, 969–973, Mar. 2010.
17. Yu, J. S. and R. C. Rudduck, "H-plane pattern of a pyramidal horn," *IEEE Trans. Antennas Propagat.*, Vol. 17, No. 5, 651–652, Sep. 1969.
18. Yu, J. S., R. C. Rudduck, and L. Peters, "Comprehensive analysis for E-plane of horn antennas by edge diffraction theory," *IEEE Trans. Antennas Propagat.*, Vol. 14, No. 2, 138–149, Mar. 1966.

19. Russo, P. M., R. C. Rudduck, and L. Peters, "A method for computing E-plane patterns of horn antennas," *IEEE Trans. Antennas Propagat.*, Vol. 13, No. 2, 219–224, Mar. 1965.
20. Balanis, C. A., "Radiation from conical surfaces used for high-speed spacecraft," *Radio Science*, Vol. 7, No. 2, 339–343, Feb. 1972.
21. Ryan, C. and L. Peters, "Evaluation of edge-diffracted fields including equivalent currents for the caustic regions," *IEEE Trans. Antennas Propagat.*, Vol. 17, No. 3, 292–298, May 1969.